Applied Thermal Engineering 31 (2011) 2749–2756

Contents lists available at ScienceDirect

Applied Thermal Engineering

journal homepage: www.elsevier.com/locate/apthermeng

Numerical study of a metal hydride heat transformer for low-grade heat recovery Simulation of a *M*H heat transformer

F.S. Yang [a], Z.X. Zhang [a,b,*], G.X. Wang [c], Z.W. Bao [a], J.C. Diniz da Costa [c], V. Rudolph [c]

[a] State Key Laboratory of Multiphase Flow in Power Engineering, Xi'an Jiaotong University, Xi'an 710049, PR China
[b] Suzhou Research Institute, Xi'an Jiaotong University, Suzhou 215123, PR China
[c] School of Chemical Engineering, The University of Queensland, Brisbane QLD 4072, Australia

ARTICLE INFO

Article history:
Received 20 February 2011
Accepted 28 April 2011
Available online 7 May 2011

Keywords:
Metal hydride
Waste heat recovery
Numerical simulation
Specific heating power

ABSTRACT

Due to the increasing demand for clean energy and improved energy utilization, the metal hydride heat transformer for low-grade heat recovery has attracted wide attentions recently. In this paper, such a system with $LaNi_5$–$LaNi_{4.7}Al_{0.3}$ pair, which is used for upgrading waste heat to a higher temperature, was investigated in detail by numerical simulation. Different from existing studies, in this investigation only ambient and waste heat sources are involved during operation of the heat transformer, which could be advantageous in many aspects. A rigorous 2-D unsteady model was developed and numerically solved by the fully implicit finite volume method (FVM). It was shown that the proposed system can achieve steady heat upgrading operation, resulting in an average temperature boost of 6.8 K using a 358 K waste heat source. The dynamic behavior of the heat transformer in three subsequent cycles was analyzed, and the measures aiming at continuous output were further discussed.

1. Introduction

In recent years, the recovery of the waste heat from industry, featured by a large amount and a low grade (the temperature is generally below 100 °C), has attracted worldwide attentions. Waste heat recovery would contribute not only to lower energy consumption, but also to less pollution and better environment. Therefore, the research and development of waste heat recovery systems is of great interest to the scientific community. Till now many technical means have been examined for these purposes, and the promising candidates are recognized as organic Rankine cycle (ORC) [1], absorption heat pump [2] and chemical heat pump [3]. The metal hydride heat pump (MHHP) is a type of chemical heat pump, in which the heat effect accompanying hydriding/dehydriding reaction is utilized. The reaction can be written as follows:

$$M + x/2 \cdot H_2 \Leftrightarrow MH_x + \Delta H \quad (1)$$

where M is a certain metal or alloy, and the product MH_x is termed metal hydride (MH). The MHHP can achieve multiple purposes, i.e. refrigeration, heat amplification or heat upgrading. It covers a wide range of operation temperatures from −50 to 400 °C. Besides, the system is reliable and environmentally benign. These advantages make it a competitive alternative in waste heat recovery. When applied for heat upgrading, the system is also called heat transformer.

Ram Gopal and Srinivasa Murthy [4] built a 1-D conjugate heat and mass transfer model for the *M*H heat transformer with $ZrCrFe_{1.4}$–$LaNi_5$ pair, which could provide useful heat at 408–418 K. According to the authors, there exists an optimum thermal conductivity for a given bed thickness and overall heat transfer coefficient, beyond which the system performance measured by coefficient of performance (COP) is hardly affected. As the temperature of the heat input increases, the COP of system tends to increase.

Kang and Yabe [5] formulated a reaction front model for the heat transformer based on *M*Hs, and a module using $LaNi_5$–$LaNi_{4.5}Al_{0.5}$ pair was considered to upgrade waste heat at 383 K to more than 400 K. The simulation results showed that the COP of system is comparable with that of absorption heat pump (~0.5). Moreover, through increasing the heat transfer coefficient and efficiency of internal heat recovery, the system performance can be further enhanced.

A series of experimental studies on the *M*H heat transformer have been carried out by the Stuttgart University in Germany, from reactor dynamic tests [6] to system construction and operation [7,8]. It was shown that a temperature boost from 130 to 200 °C is

* Corresponding author. State Key Laboratory of Multiphase Flow in Power Engineering, Xi'an Jiaotong University, Xi'an 710049, PR China. Tel./fax: +86 29 82660689.
E-mail address: zhangzx@mail.xjtu.edu.cn (Z.X. Zhang).

1359-4311/$ – see front matter © 2011 Elsevier Ltd. All rights reserved.
doi:10.1016/j.applthermaleng.2011.04.047

Nomenclature

A	parameter in P–C–T equation
B	parameter in P–C–T equation, K
C_p	specific heat capacity at constant pressure, J kg^{-1} K^{-1}
C_v	specific heat capacity at constant volume, J kg^{-1} K^{-1}
E	activation energy, J mol^{-1}
h	convective heat transfer coefficient, W m^{-2} K^{-1}
ΔH	reaction heat, J mol^{-1} H_2
$[H/M]$	hydrogen to metal ratio
k	reaction rate constant, s^{-1}
K	permeability, m^2
$\dot{m}$	mass source term of reaction, kg m^{-3} s^{-1}
M	molecular weight, kg mol^{-1}
N	amount, mol
P	pressure, Pa
q	mass flow rate, kg s^{-1}
Q	heat, J
r	r-coordinate, m
R_g	general gas constant, J mol^{-1} K^{-1}
S	area, m^2
t	time, s
T	temperature, K
$\vec{U}$	gas velocity, m s^{-1}
V	volume, m^3
W	mass, kg
X	reacted fraction
z	z-coordinate, m

Greek symbols

β	hysteresis factor in P–C–T equation
ε	volume fraction
λ	thermal conductivity, W m^{-1} K^{-1}
μ	dynamic viscosity, Pa s
ρ	density, kg m^{-3}
ϕ	plateau flatness factor in P–C–T equation
ϕ_0	plateau flatness factor in P–C–T equation
ψ	fraction of transferred hydrogen

Subscripts

a	absorption or hydriding
Al	Aluminum foam
b	bulk bed
c	connecting volume
d	desorption or dehydriding
e	equilibrium
eff	effective
f	heat transfer fluid
F	final
g	hydrogen gas
H	high
I	initial
in	inlet or input
L	low
M	intermediate
MH	metal hydride
out	outlet or output
sat	saturated
v	void
w	vessel wall

viable for a two-stage MHHP system adopting 3 misch metal–nickel alloys, which is potentially applicable in many industrial processes, e.g. rectification of oil products. However, the system performance concerning thermal efficiency was not quite satisfactory, especially after the shutting down of internal heat recovery due to operation failure.

Liang et al. [9] presented a thermodynamic model for MH heat transformer, through which the main factors affecting system performance were discussed. Enhanced heat transfer and compact reactor design were found to be necessary to achieve satisfactory COP. Besides, the influence of operation conditions, e.g. the temperature of driving heat source, was also very important.

Meng et al. [10] proposed a novel liquefied natural gas (LNG) cold energy recovery system, in which an MH based heat transformer was integrated to reduce the overall energy consumption. Based on the results of thermodynamic analysis, the authors pointed out that the improvement of heat transformer performance is crucial for optimization of the whole cold energy recovery system.

Although a number of studies have been carried out both theoretically and experimentally, the MH-based heat transformers concerned are basically similar: at least three heat sources (or sinks) of varied temperatures have to be used for operation, which results in a complicated system construction. Moreover, the COP and specific heating power (SHP) are not quite satisfactory. In this paper, a single stage system using $LaNi_5$–$LaNi_{4.7}Al_{0.3}$ pair was considered, where the high temperature heat sink was simply replaced by the waste heat. A rigorous mathematical model for system operation was established, in which some factors neglected in previous studies, e.g. the effect of vessel wall, the reaction during sensible heating/cooling processes, were taken into account. Through numerical simulation, the working characteristics of the system in repeated cycles were explored and the performance of the novel system was assessed.

2. Mathematical model

2.1. Operation principle

A single stage MH heat transformer was considered. It is composed of at least two reactors coupled by the hydrogen pipeline, as is shown in Fig. 1a. Two kinds of MHs, say M_1 and M_2, are packed respectively in the reactors. A general working cycle proceeds in 4 sub-processes as described below, and the corresponding thermodynamic cycle was shown in Fig. 1b.

In recharging or regeneration period (Sub-process 1), the on–off valve of hydrogen pipeline is kept open, and hydrogen flows from metal hydride M_1 (at State 2) to M_2 (at State 3), driven by the difference of equilibrium pressures. Heat at intermediate temperature T_M, namely waste heat, is supplied to M_1 through certain fluid for hydrogen desorption, while M_2 rejects absorption heat at ambient temperature T_L.

In pre-heating period (Sub-process 2), the on–off valve is kept closed. The reactor packed with M_1 is sensibly heated to the high temperature T_H (from State 2 to State 1), meanwhile the other reactor packed with M_2 is sensibly heated to T_M (from State 3 to 4).

In working period (Sub-process 3), the on–off valve is kept open and hydrogen reversely flows from M_2 (at State 4) to M_1 (at State 1). Waste heat is supplied to M_2 for hydrogen desorption, while the

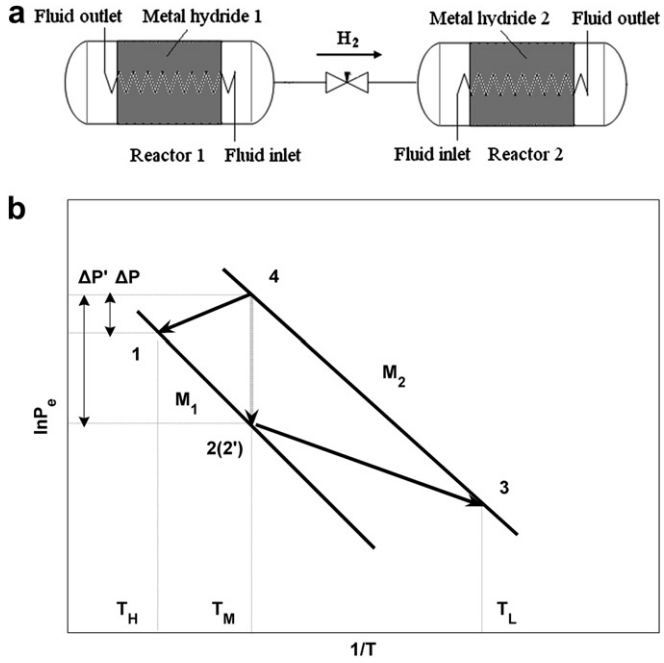

Fig. 1. MH heat transformer (a): Schematic (b): Thermodynamic cycle in the Clapeyron diagram.

absorption of hydrogen in M_1 generates the useful output at high temperature T_H. Thus the heating is achieved.

In pre-cooling period (Sub-process 4), the on–off valve is kept closed. The reactors packed with M_1 and M_2 are sensibly cooled to T_M (from State 1 to State 2) and T_L (from State 4 to State 3), respectively. To this point, the whole working cycle is completed.

The introduction of a heat sink at T_H, however, is an issue deserves careful thinking. Firstly, it may add to the difficulty of constructing a system, because there has to be some proper heat sink nearby, and another fluid may be involved as the medium. Besides, during Sub-process 3 the driving force of reaction (i.e. the pressure difference ΔP) is limited. Meanwhile the temperature difference between T_M and T_H suggests corresponding sensible heat loss. Hence the above-mentioned system can hardly provide satisfactory performance.

To resolve these problems, the idea of MH based air conditioning system was borrowed, for which the ambient air is used as both heat source and sink [11,12]. In this investigation, the waste heat fluid plays a similar role. As can be seen in Fig. 1b, at the State 2′ waste heat is introduced as the heat sink and the new cycle 2–3–4–2′–2 can be formed. The pressure difference as the driving force of reaction ($\Delta P'$) tends to increase in the working period, thus enhanced reaction rate will lead to short cycle time, which is desirable for larger output power. This is particularly suitable for the hydride pair providing just a moderate driving force for Sub-process 3. Moreover, because of the temperature change fluid experiences during hydriding/dehydriding reaction, an actual heat upgrading can still be achieved, as will be illustrated later.

2.2. Mathematical model

The ambient and waste heat temperatures were respectively specified as 293 and 358 K, and the pair $LaNi_5$–$LaNi_{4.7}Al_{0.3}$ was selected for use according to a procedure proposed by the authors [13].

In the application of MH systems, the tubular type reactor was considered here as it is widely used [14]. The dimension of the reactor is shown in Fig. 2. Aluminum foam was supposed to be inserted in the MH bed for enhanced heat transfer, while tube wall was made of stainless steel. The following assumptions were made to formulate the model:

1) The physical properties of the reaction bed are constant during the reaction.
2) The gas phase (hydrogen) is ideal from the thermodynamic view.
3) There is no temperature slip between the solid phase and the gas phase, which is also termed “local thermal equilibrium”.
4) The radiative heat transfer is neglected due to the moderate temperature range to be modeled.
5) When the valve between coupling reactors is open (referring to Fig. 1a), simultaneous thermodynamic equilibrium can be achieved.
6) The state of hydrogen is uniform in the connecting volume.

When the two reactors are connected (Sub-processes 1 and 3), hydriding reaction occurs in one reactor while dehydriding occurs in the other. The modeling equations for the two reactors are basically similar and thus only one set of the equations for reactor 1 packed with $LaNi_5$ is discussed as follows.

Continuity equation for hydrogen gas can be expressed by:

$$\frac{\partial \varepsilon_v \rho_g}{\partial t} + \nabla\left(\rho_g \vec{U}\right) = -\dot{m}\cdot M_g \tag{2}$$

Mass equation for the MH can be written as follows:

$$\frac{\partial \varepsilon_{MH}\rho_{MH}}{\partial t} = \dot{m}\cdot M_g \tag{3}$$

Unlike previous investigations, the local reaction state was not assumed beforehand while determined according to the actual pressure and equilibrium pressure, giving:

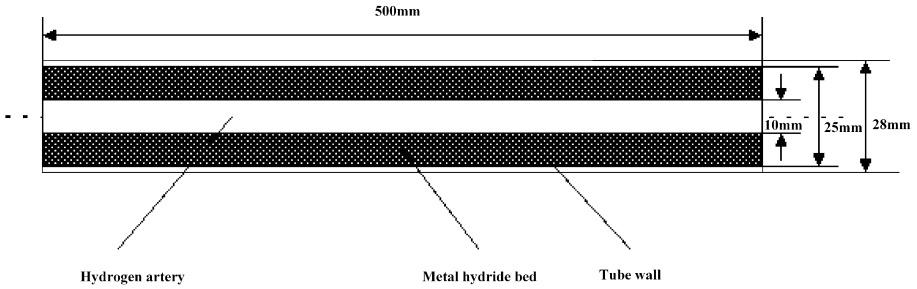

Fig. 2. The dimension of the tubular reactor for investigation (mm).

$$\dot{m} = \frac{\varepsilon_{MH}\cdot\rho_{MH}}{M_{MH}}\cdot[\mathrm{H}/M]_{sat}\cdot\left(\max\left(0,\ (P_g-P_{e,a})\right)\cdot\frac{\mathrm{d}X}{\mathrm{d}t}\Big|_a + \max\left(0,\ -(P_g-P_{e,d})\right)\cdot\frac{\mathrm{d}X}{\mathrm{d}t}\Big|_d\right) \quad (4)$$

Momentum equation for hydrogen gas is described by:

$$\vec{U} = K/\mu\cdot\nabla P_g \quad (5)$$

Energy equations for the bulk bed including both solid and gas phases are given by:

$$\frac{\partial\left(\sum\varepsilon_i\rho_i C_{pi}\right)T_b}{\partial t} + \nabla\cdot\left(\rho_g C_{pg}\vec{U}T_b\right) = \nabla\left(\lambda_{\mathrm{eff}}\nabla T_b\right) + \dot{m}\cdot\Delta\mathrm{H} \quad (6)$$

The hysteresis and plateau slope were taken into account in the P–C–T equation used [15]:

$$P_{e,a} = \exp\left(-A/T_b + B + (\phi-\phi_0)\cdot\tan\left(\pi^*\times(X-1/2)\right) + \beta/2\right) \quad (7a)$$

$$P_{e,d} = \exp\left(-A/T_b + B + (\phi-\phi_0)\cdot\tan\left(\pi^*\times(X-1/2)\right) - \beta/2\right) \quad (7b)$$

Reaction kinetic equations for absorption/desorption take the form of one-order chemical reaction [16,17]:

$$\frac{\mathrm{d}X}{\mathrm{d}t}\Big|_a = k_a\ \exp\left(-E_a/(R_g T_b)\right)\ \ln\left(P_g/P_{e,a}\right)(1-X) \quad (8a)$$

$$\frac{\mathrm{d}X}{\mathrm{d}t}\Big|_d = k_d\ \exp\left(-E_d/(R_g T_b)\right)\cdot\left((P_{e,d}-P_g)/P_{e,d}\right)\cdot X \quad (8b)$$

The equations for reactor 2 can be written likewise and are skipped here. The state of gas in the connecting volume was renewed with time marching:

$$\frac{\mathrm{d}N_c}{\mathrm{d}t} = -\left(\int\rho_{g1}\vec{U}_1\mathrm{d}S_1 + \int\rho_{g2}\vec{U}_2\mathrm{d}S_2\right)\Big/M_g \quad (9)$$

$$\frac{\mathrm{d}N_c C_{vg}T_c}{\mathrm{d}t} = -\left(\int\rho_{g1}C_{pg}\vec{U}_1T_1\mathrm{d}S_1 + \int\rho_{g2}C_{pg}\vec{U}_2T_2\mathrm{d}S_2\right)\Big/M_g \quad (10)$$

$$P_cV_c = N_cR_gT_c \quad (11)$$

Therefore, the boundary conditions for both reactors are actually transient. When the two reactors are disconnected (Sub-processes 2 and 4), some authors approximate the process as simple heat transfer with no reaction [4,18], and only Eq. (6) eliminating the reaction source term is adopted. However, during this time pressure may vary in a large range and trigger the reaction, thus such simplification is questionable. In this paper, the full set of equations, i.e. Eqs. (2)–(8), were still used to simulate Sub-process 2 and 4, thereby local reaction is allowed to occur. However, in this case one reactor is isolated from the other, and mass/heat exchange occurs between one reactor bed and half of the connecting volume. The equations can be written following the expression of Eqs. (9)–(11).

2.3. Initial and boundary conditions

Uniform reacted fraction, temperature and pressure were assumed in reactors 1 (packed with $LaNi_5$) and 2 (packed with $LaNi_{4.7}Al_{0.3}$) initially, and the equilibrium state was reached. The initial reacted fraction of reactors 1 and 2 are 0.2 and 0.8, respectively. The ambient temperature T_L is 293 K and the waste heat temperature T_M is 358 K. As shown in Table 1, the initial state of the latter sub-process is exactly the final state of the former sub-process.

For a tubular reactor, three types of boundary conditions can be classified according to Yang et al. [19], details are referred to the original paper. The convective heat transfer coefficient is 1500 W/(m K) and the number of heat transfer unit (NTU) is 1. Water and oil were used as the heat transfer fluids for low and high temperatures, respectively.

Trial computation was done to determine the time for the 4 sub-processes t_1, t_2, t_3, t_4 as 542, 120, 240 and 80 s, under which condition a sufficient amount of hydrogen (60% of total inventory) could be transferred between the reactors.

2.4. Numerical technique

The model was solved by a classical finite volume method (FVM) [20], through which the heterogeneous and distributed physical properties can be dealt with easily. The computation domain includes both *M*H bed and the vessel wall, while the same set of governing equations was applied in the whole domain. However, the physical properties in respective regions are varied as shown in Table 2. Obviously, owing to the appropriate properties settings, the governing equations automatically degenerate into simple heat conduction in the region of vessel wall, thus the effect of vessel wall is considered in the simulation without changing the general solution procedure. The P–C–T and kinetic parameters in simulation are referred to the original papers [15–17]. The time step was 0.01 s and a 20 × 12 grid was proved to provide enough accuracy. Convergence was assumed when the error of P and T are respectively lower than 1×10^{-3} Pa and 1×10^{-3} K.

3. Results and discussion

3.1. Numerical validation

The experimental data reported in an open literature [21] was used for the validation of the model developed in this study. In the

Table 1
The settings of operation conditions for the MH heat transformer.

Sub-process	Parameters	Reactor 1	Reactor 2
Regeneration	Fluid inlet temperature	T_L	T_M
	Initial reacted fraction	0.2	0.8
	Initial temperature	T_L	T_M
	Duration	t_1	
Pre-heating	Fluid inlet temperature	T_M	T_M
	Initial reacted fraction	The ending state of Sub-process 1	The ending state of Sub-process 1
	Initial temperature	The ending state of Sub-process 1	The ending state of Sub-process 1
	Duration	t_2	
Working	Fluid inlet temperature	T_M	T_M
	Initial reacted fraction	The ending state of Sub-process 2	The ending state of Sub-process 2
	Initial temperature	The ending state of Sub-process 2	The ending state of Sub-process 2
	Duration	t_3	
Pre-cooling	Fluid inlet temperature	T_L	T_M
	Initial reacted fraction	The ending state of Sub-process 3	The ending state of Sub-process 3
	Initial temperature	The ending state of Sub-process 3	The ending state of Sub-process 3
	Duration	t_4	

Table 2
The physical properties of the reaction bed and vessel wall.

	Reaction bed	Vessel wall
Volume fraction of gas ε_g	0.438	10^{-5}
Volume fraction of MH ε_{MH}	0.462	0
Volume fraction of Al foam ε_{Al}	0.1	0
Volume fraction of wall material ε_w	0	0.99999
Thermal conductivity λ, W m^{-1} K^{-1}	7.5	13.3 (stainless steel)
Permeability K, m^2	10^{-12}	10^{-30} (basically impermeable)

experiment reported by the literature, tubular reactors were also applied and $MmNi_{4.5}Al_{0.5}$–$MmNi_{4.2}Al_{0.1}Fe_{0.7}$ pair was used. The detailed design and operation conditions were described and will not be elaborated here. As shown in Fig. 3, for both transferred amount of hydrogen and the temperature, the simulation results of our model agree with the experimental results well, thus the accuracy of the model was proved.

3.2. Cyclic behavior

In this study, three subsequent cycles were simulated to explore the dynamic behavior of the proposed heat transformer system.

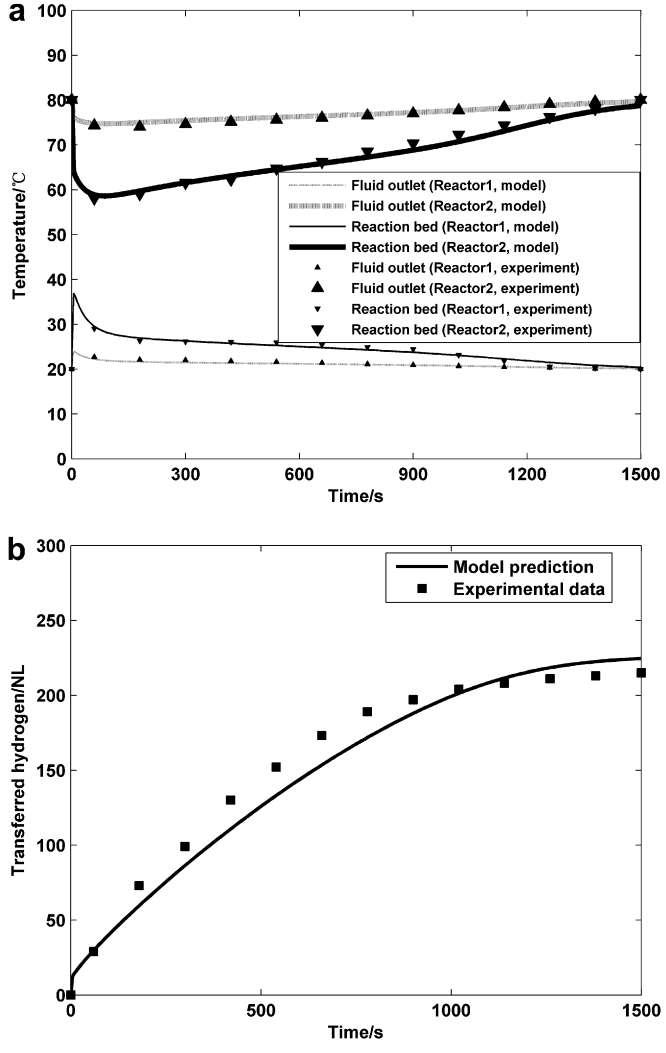

Fig. 3. The comparison of simulated results and the experimental data (a): Hydrogen amount transferred (b): Temperature.

The temporal profiles of average reacted fraction in the coupling reactors were shown in Fig. 4, where the 4 Sub-processes were respectively indexed by 1, 2, 3 and 4. The profiles appear to be repeated in a cyclic manner, which resemble those reported by Paya et al. [22] through experimental investigation.

It is noteworthy that after one period of operation, the initial conditions for the latter cycle are not exactly the same as those for the former, see Fig. 5. However, such deviation tends to get smaller and smaller as cycle number increases. The difference between cycle 1 and cycle 2 is still remarkable, while cycle 3 has been very close to cycle 2. The asymptotic phenomena should be attributed to the fixed operation settings for all cycles, i.e. operation time for Sub-processes, fluid flow rate and temperature. Therefore, it could be concluded that a steady operation, both in lumped and distributed sense, can be attained in a few cycles under the given conditions.

During Sub-processes 1 and 3, hydriding and dehydriding reactions occur respectively in the two reactors, the average reacted fraction in a certain reactor varies in a wide range from 0.2 to 0.8, as can be seen in Fig. 4. During Sub-processes 2 and 4, small variation in the average reacted fraction was observed for reactor 1, which proves the minor reaction occurring and supports using the full set of equations in simulation. As for reactor 2, the variation of reacted fraction during Sub-processes 2 and 4 is hardly discernible.

Although Sub-processes 2 and 4 take relatively short time and no significant reaction occurs, the temperature of the reactor, especially reactor 1 packed with $LaNi_5$, changes drastically. As shown in Fig. 6, in the interval of 120 s for Sub-process 2, the bed temperature approaches to 358 K from an initial temperature of around 298 K. Moreover, we can see that the temperature distribution in the reactor is quite uniform throughout the Sub-process, which should be largely attributed to the enhanced heat transfer by aluminum foam.

The temporal profiles of fluid outlet temperature in the coupling reactors were respectively shown in Fig. 7. During Sub-process 3, the outlet fluid of reactor 2 has higher temperature than the input waste heat and is utilized as the output. The temperature of heat output varies with time. It climbs to a peak value of 368.4 K soon after Sub-process 3 commences, which achieves a temperature boost of 10.4 K. After that the outlet temperature falls down to around 362 K slowly. The average gain in temperature during the output is 6.8 K. The above result proves our view that usable heat upgrading effect can still be realized adopting the proposed system.

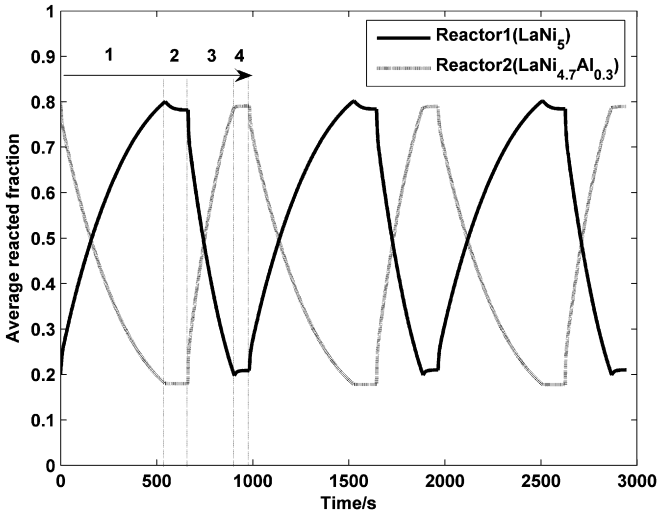

Fig. 4. The temporal profiles of average reacted fraction for the coupling reactors.

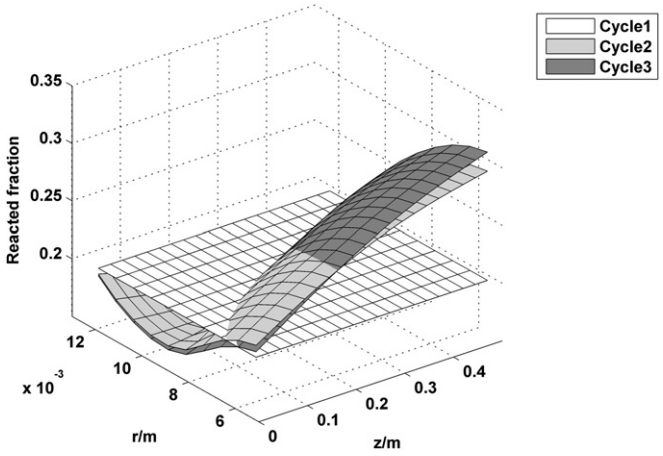

Fig. 5. The initial reaction distribution in reactor 1 for the first 3 cycles.

The temporal profiles of pressure in the reactors 1 and 2 were shown in Fig. 8. As can be seen, when the valve is opened after Sub-processes 2 or 4, large pressure differences are formed between the reactors as driving force of the reaction, then a common pressure is reached simultaneously. Obviously, the initial driving force of reaction during Sub-process 3 is much larger than that during Sub-process 1, as indicated in Fig. 8. This explains why Sub-process 1 takes longer time than Sub-process 3 does for a certain amount of hydrogen to be transferred.

3.3. Continuous output

For a realistic *M*H heat transformer system, it is favorable that Sub-processes 1 and 3 match each other in operation time, so that two pairs of coupling reactors can provide semi-continuous output in turn. Therefore, the system should be adapted somehow to meet this requirement. Three possible solutions are summarized as follows:

1) A new pair of alloys is selected instead of $LaNi_5$—$LaNi_{4.7}Al_{0.3}$, which can achieve more balanced reaction driving forces during Sub-process 1 and 3 under the given conditions. The measure is less easy to implement because the design of the system should be changed completely.
2) The temperatures of heat sources are varied, i.e. increasing T_M or decreasing T_L. As can be seen in Fig. 1b, the reaction driving force for Sub-process 1 will be increased correspondingly, which causes t_1 to shorten and approach t_3.

   In this paper, the waste heat at 363 and 368 K were also supposed to be used as the input, and corresponding simulations were conducted for the proposed system. It was found that in either case t_1 is shortened while t_3 is almost constant. When utilizing 368 K waste heat, t_1 and t_3 were respectively determined as 360 and 224 s, which does show better symmetry. Meanwhile, heat output at a temperature higher than 373 K can be provided during most time in Sub-process 3, as is seen in Fig. 9. In other words, it is possible to produce ambient pressure steam simply using 368 K waste heat, which shows certain potential for industrial application.
3) The mass flow rate of fluid for a certain Sub-process is varied. Unlike the former two measures, this one is of more dynamic sense.

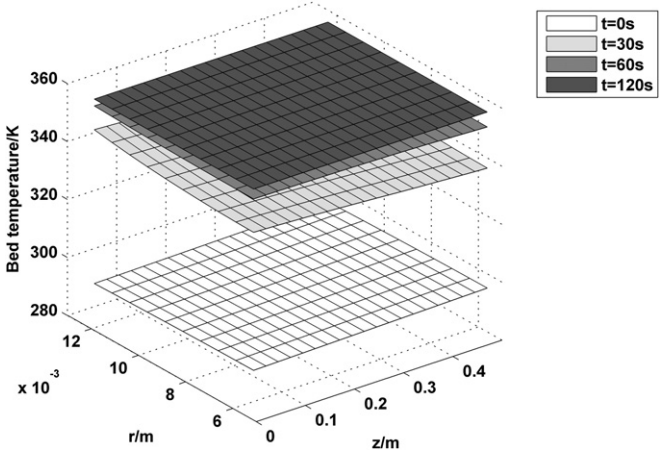

Fig. 6. The variation of bed temperature in reactor 1 during Sub-process 2.

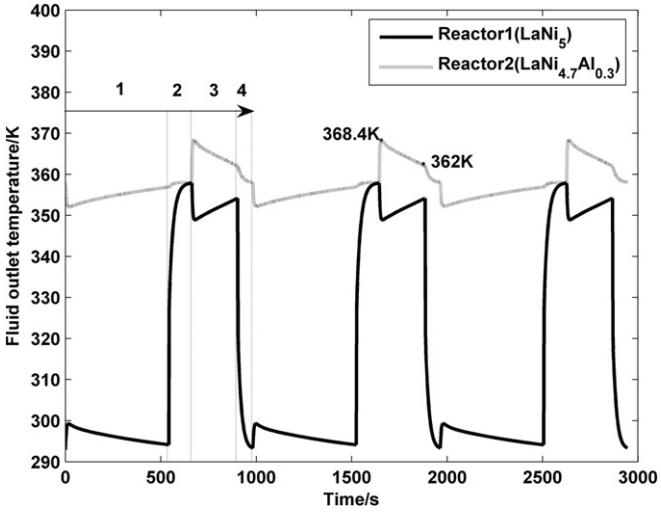

Fig. 7. The temporal profiles of fluid outlet temperature for the coupling reactors.

During the hydriding/dehydriding reaction, the bed temperature experiences change and thus the reaction driving force, which often takes the form of equilibrium pressure difference between

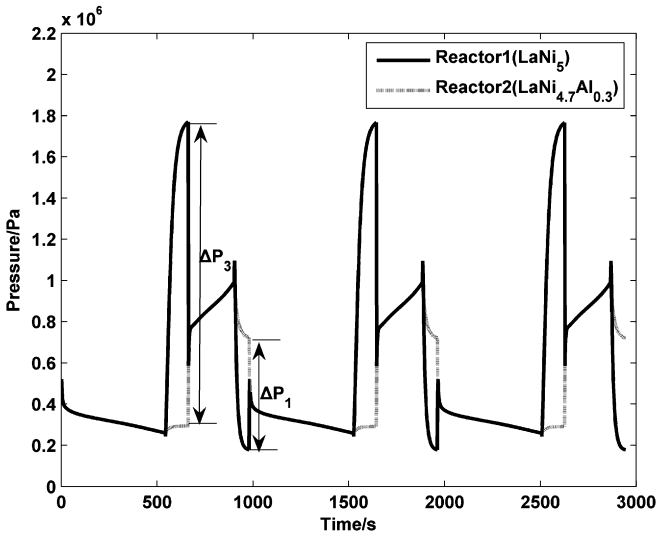

Fig. 8. The temporal profiles of pressure in the coupling reactors.

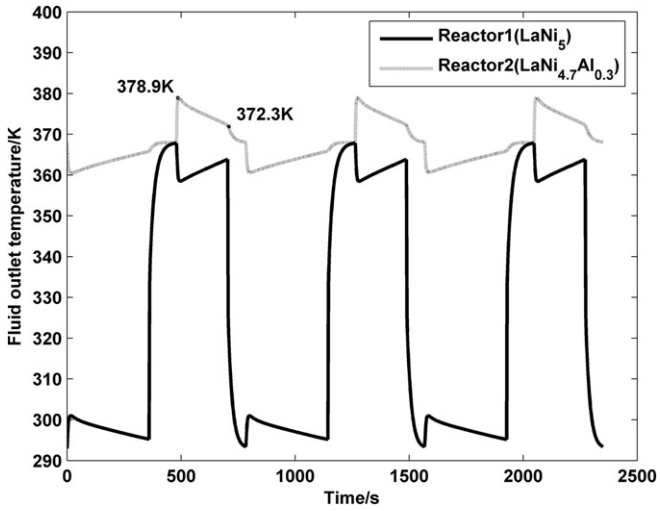

Fig. 9. The temporal profiles of fluid outlet temperature for the coupling reactors with 368 K waste heat input.

coupling reactors, is not constant. If the heat exchange between the reaction bed and heat transfer fluid is effective, the bed temperature can be kept close to the fluid temperature. This suggests that there is a stable large driving force of reaction. On the contrary, poor heat exchange will inevitably lead to smaller driving force of reaction and prolonged operation time.

According to the general heat transfer principles, the convection heat transfer coefficient h for incompressible fluid increases with its velocity (or mass flow rate), which can be simply expressed as follows:

$$h \propto q_f^{\alpha} \tag{12}$$

where α is between 0 and 1 [23]. Without losing generality, a moderate value of 0.5 is taken for discussion. The mass flow rate for both reactors was reduced by 50% during Sub-process 3, and the corresponding system operation was simulated. As can be expected, t_1 is kept constant while t_3 increases up to 322 s, an improved match was obtained. Moreover, due to the reduced mass flow rate, the temperature boost is also increased, as can be seen in Fig. 10. The peak value reaches 14.7 K and an average gain in temperature of

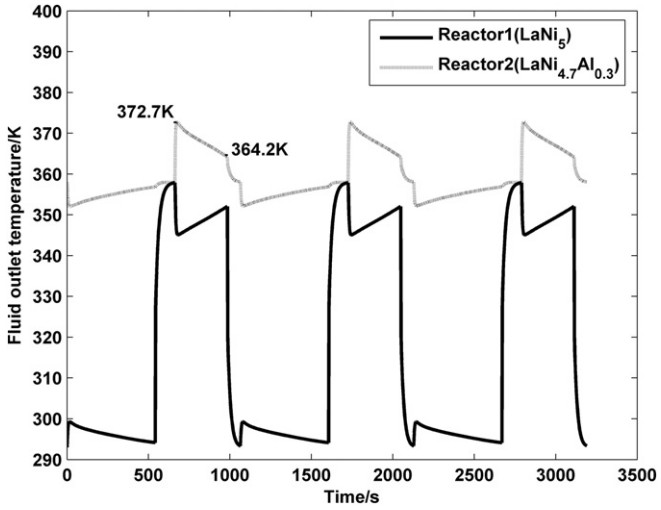

Fig. 10. The temporal profiles of fluid outlet temperature for the coupling reactors with reduced fluid flow rate.

10.1 K can be realized. It is noteworthy that the above effect may be larger or smaller as α varies, yet the qualitative trend should hold.

3.4. System performance

In the assessment of *M*H heating/cooling systems, the coefficient of performance (COP) and the specific output power concerning alloy mass, the two most commonly used indices, are crucial. COP is defined as the useful heat output versus the input in a cycle period:

$$\mathrm{COP} = \frac{Q_{\mathrm{out}}}{Q_{\mathrm{in}}} \tag{13}$$

As has been shown above, the mass flow rate of the heat transfer fluid is fixed while its outlet temperature varies with time. Therefore, the heat input and output can be obtained by integration of the fluid temperature profiles, giving:

$$Q = \int_{t=t_I}^{t_F} q_f C_{pf} (T_{\mathrm{out}}(t) - T_{\mathrm{in}}) \mathrm{d}t \tag{14}$$

where t_I and t_F are the initializing and ending moment of a Sub-process, T_{in} is the fixed inlet temperature while T_{out} is the time-varying outlet temperature. It should be noted that the calculated Q is the heat quantity actually exchanged between the fluid and reaction bed, thus is the net input or output with sensible heat loss considered. Because the simulation results were stored discretely, numerical integration was implemented to calculate Q.

For *M*H based cooling systems, specific cooling power is often used to measure system performance [11,12,24]. Similarly, the specific heating power (SHP) can be defined for a heat transformer:

$$\begin{aligned} \mathrm{SHP} &= \frac{Q_{\mathrm{out}}}{(W_{MH_1} + W_{MH_2}) \sum t} \\ &= \frac{Q_{\mathrm{out}}}{(W_{MH_1} + W_{MH_2})(t_1 + t_2 + t_3 + t_4)} \end{aligned} \tag{15}$$

where the hydride mass (W_{MH}) could be determined from the design conditions of the reactors.

For the basic case of simulation, the average output power in a cycle was calculated to be 0.109 kW. The system can be scaled up simply by using more tubular modules. For the first cycle, the COP was determined to be 0.407, and the value kept almost constant for the following cycles (0.409, 0.409). The COP for the proposed system, which takes into account the sensible heat loss resulting from tube wall and Al foam in calculation, is close to that reported by Kang and Yabe [5], while a bit larger than that from Ram Gopal and Srinivasa Murthy [4]. The latter comparison result may be due to the different operation conditions.

As for the SHP, its value was calculated to be 70.5 W/kg, higher than the reported SHP through theoretical or experimental studies [5]. It is well known that a large SHP suggests better economy. Therefore, the proposed system shows certain superiority in this aspect.

In summary, the system newly presented in this study exhibits competitive performance concerning COP and SHP, even though no internal heat recovery is carried out yet and the indices are still under-optimum.

4. Conclusions

In this paper, a modified metal hydride heat transformer system was proposed, for which waste heat fluid serves as both heat source and heat sink. A 2-D mathematical model was developed to

simulate the system for optimization and enhancement of the system design. The cyclic operation of the heat transformer was numerically analyzed and following conclusions can be drawn:

1) Steady useful heat output is provided by the proposed system. Using 358 K waste heat source, an average gain of 6.8 K in temperature has been achieved.
2) The proposed system can be further improved in order to realize continuous output. The most effective measures for improvement include adopting new pairs of alloys, adapting temperature of heat sources, and varying the fluid flow rate.
3) The performance of the proposed system is acceptable for thermal energy recovery from a low-grade (the temperature is generally below 100 °C) waste sources. Even though the sensible heat loss was fully considered, the system COP is as high as 0.407 and SHP reaches 70.5 W/kg, which are comparable with or even superior to the reported performances of existing metal hydride heat transformer systems.

Acknowledgments

The financial support from the Ph D Program Foundation of Chinese Education Ministry (No.20100201110007), the Application Fundamentals Research Program of Suzhou City (No.SYG201019) are greatly acknowledged by the authors from Xi'an Jiaotong University.

References

[1] T.C. Hung, T.Y. Shai, S.K. Wang, A review of organic Rankine cycles (ORCs) for the recovery of low grade heat, Energy 22 (1997) 661–667.
[2] V. Tufano, Heat recovery in distillation by means of absorption heat pumps and heat transformers, Appl. Therm. Eng. 17 (1997) 171–178.
[3] S. Spoelstra, W.G. Haije, J.W. Dijkstra, Techno–economic feasibility of high-temperature high-lift chemical heat pumps for upgrading industrial waste heat, Appl. Therm. Eng. 22 (2002) 1619–1630.
[4] M. Ram Gopal, S. Srinivasa Murthy, Prediction of metal hydride heat transformer performance based on heat transfer and reaction kinetics, Ind. Eng. Chem. Res. 34 (1995) 2305–2313.
[5] B.H. Kang, A. Yabe, Performance analysis of a metal hydride heat transformer for waste heat recovery, Appl. Therm. Eng. 16 (1996) 677–690.
[6] R. Werner, M. Groll, Two-stage metal hydride heat transformer laboratory model: results of reaction bed tests, J. Less-Common Met. 172–174 (1991) 1122–1129.
[7] A. Isselhorst, M. Groll, Two-stage metal hydride heat transformer laboratory model, J. Alloys Compd. 231 (1995) 888–894.
[8] E. Willers, M. Groll, The two-stage metal hydride heat transformer, Int. J. Hydrogen Energy 24 (1999) 269–276.
[9] B. Liang, Z.X. Zhang, Y.Q. Wang, Performance analysis to metal hydride heat pumps for heat upgrading, J. Xi'an Jiaotong Univ. 38 (2004) 89–92.
[10] X.Y. Meng, F.F. Bai, F.S. Yang, Z.W. Bao, Z.X. Zhang, Study of integrated metal hydrides heat pump and cascade utilization of liquefied natural gas cold energy recovery system, Int. J. Hydrogen Energy 35 (2010) 7236–7245.
[11] S.G. Lee, Y.K. Kim, J.Y. Lee, Operating characteristics of metal hydride heat pump using Zr-based laves phases, Int. J. Hydrogen Energy 20 (1995) 77–85.
[12] F. Qin, J.P. Chen, M.Q. Lu, Z.J. Chen, Y.M. Zhou, K. Yang, Development of a metal hydride refrigeration system as an exhaust gas-driven automobile air conditioner, Renew. Energy 32 (2007) 2034–2052.
[13] F.S. Yang, X.Y. Meng, Z.X. Zhang, Y.Z. Yu, Selection of alloys in a metal hydride heat pump – a new procedure, In: Proceedings of International Refrigeration and Air Conditioning Conference at Purdue, West Lafayette, USA, 2008.
[14] F.S. Yang, G.X. Wang, Z.X. Zhang, X.Y. Meng, V. Rudolph, Design of the metal hydride reactor – a review on the key technical issues, Int. J. Hydrogen Energy 35 (2010) 3832–3840.
[15] T. Nishizaki, K. Miyamoto, K. Yoshida, Coefficients of performance of hydride heat pumps, J. Less-Common Met. 89 (1983) 559–566.
[16] A. Jemni, S. Ben Nasrallah, Study of two-dimensional heat and mass transfer during absorption in a metal-hydrogen reactor, Int. J. Hydrogen Energy 20 (1995) 43–52.
[17] A. Jemni, S. Ben Nasrallah, Study of two-dimensional heat and mass transfer during desorption in a metal-hydrogen reactor, Int. J. Hydrogen Energy 20 (1995) 881–891.
[18] A. Satheesh, P. Muthukumar, A. Dewan, Computational study of metal hydride cooling system, Int. J. Hydrogen Energy 34 (2009) 3164–3172.
[19] F.S. Yang, X.Y. Meng, J.Q. Deng, Y.Q. Wang, Z.X. Zhang, Identifying heat and mass transfer characteristics of metal-hydrogen reactor during adsorption – parameter analysis and numerical study, Int. J. Hydrogen Energy 33 (2008) 1014–1022.
[20] W.Q. Tao, Numerical Heat Transfer (In Chinese), second ed. Xi'an Jiaotong University Press, Xi'an, 2001.
[21] H. Bjurstrom, Y. Komazaki, S. Suda, The dynamics of hydrogen transfer in a metal hydride heat pump, J. Less-Common Met. 131 (1987) 225–234.
[22] J. Paya, M. Linder, E. Laurien, J.M. Corberan, Dynamic model and experimental results of a thermally driven metal hydride cooling system, Int. J. Hydrogen Energy 34 (2009) 3173–3184.
[23] S.M. Yang, W.Q. Tao, Heat Transfer (In Chinese), fourth ed. High Education Press, Beijing, 2006.
[24] M. Linder, R. Mertz, E. Laurien, Experimental results of a compact thermally driven cooling system based on metal hydrides, Int. J. Hydrogen Energy 35 (2010) 7623–7632.